Progress In Electromagnetics Research B, Vol. 118, 135–152, 2026 PIER B

(Received 16 April 2026, Accepted 11 September 2026, Scheduled 26 September 2026)

Review of Radar Absorbers: From Classical Salisbury Screens to Intelligent Tunable and Reconfigurable Radar Absorbers

V. P. Inbavalli[1,*], T. R. Suresh Kumar[2], P. Prakasam[2], and K. S. Preetha[2]

[1] *Independent Researcher, Vellore, Tamil Nadu, India*
[2] *School of Electronics Engineering, Vellore Institute of Technology, Vellore, Tamil Nadu 632014, India*

ABSTRACT: Electromagnetic absorbers are specially designed structures that absorb electromagnetic waves incident on their surface and reduce reflections in a specified frequency range. They are used within a wide range of applications, including stealth technology, reduction of electromagnetic radiation, and electromagnetic compatibility. This paper provides a comprehensive review of radar absorber design techniques, starting with basic homogeneous resistive sheet-based absorbers and progressing to advanced designs incorporating resistive frequency-selective surfaces. A separate detailed review is carried out on transparent absorbers designed for the optical transparency requirement in canopies and windows. Focus is given to the recent development of tunable absorbers designed to control resistive and reactive characteristics using an active element to tune various parameters that pertain to absorption. This paper summarizes key approaches for achieving narrowband, broadband, ultra-wideband, multiband, polarization-insensitive, and wide-incidence-angle absorption. Recent advancements and technical challenges in absorber design, such as low profile, flexibility, transparency, and real-time tunability, are systematically reviewed to guide future innovations in radar absorber technology.

1. INTRODUCTION

Electromagnetic (EM) radar absorbers are designed to reduce the radar cross-section (RCS) of a conducting structure. During World War II, to improve radar performance and reduce detectability, absorbers were designed. Absorbers are mounted on the surface of objects to reduce RCS achieved by providing a non-reflective surface for EM waves by reducing the reflections of incident EM waves. The primary objective of radar absorbers is to enhance their stealth by reducing targets' RCS. In addition to stealth applications, radar absorbers are extensively used in the mitigation of undesirable EM radiation, EMC, wireless energy harvesting, and other applications that require the control of EM propagation. Absorbers can absorb EM waves within a specific frequency range by impedance matching technique, which is determined by the design and material used.

Several review articles on electromagnetic absorbers have been reported in the literature, but most of them focus on specific absorber categories, including metamaterial absorbers, frequency-selective surface (FSS) based absorbers, transparent absorbers, and tunable absorbers. In contrast, this review presents a unified perspective, covering the complete evolution of radar absorber technologies, beginning with classical quarter-wavelength absorbers and extending to contemporary intelligent and reconfigurable absorber designs. The proposed review paper summarizes recent developments in absorber technology and critically compares different absorber technologies in bandwidth, profile thickness, fabrication complexity, angular stability, polarization sensitivity, transparency, tunability, and practical design trade-offs. The review paper also comprehensively discusses recent research trends, including flexible absorbers, screen-printed absorbers, transparent absorbers, three-dimensional absorbers, adaptive intelligent tunable absorbers, and AI-assisted design. Consequently, the proposed review article not only serves as a survey of existing literature, but it will also be a design-oriented reference for researchers working on next-generation radar absorber technologies.

The electromagnetic waves incident on an absorber may be from any direction, with arbitrary polarizations, and across any frequency band. With the unpredictable nature of the EM source, achieving an impedance-matching surface is a challenge. Requirements in the absorber design are a thinner profile, a wider absorption bandwidth, and stable absorption for varying polarization and incidence angle. Figure 1 illustrates layers used in constructing a radar absorber and challenges involved in the design, requirements, and applications of an EM absorber. A basic form of radar absorber consists of three layers, viz., (i) a perfect electric conductor (PEC): a metallic ground plane to suppress any transmission or back radiation, (ii) dielectric layer: quarter-wavelength ($\lambda/4$) spacer that decides the operating frequency, and (iii) lossy resistive layer(s): key component for energy loss.

1.1. Classification of Radar Absorbers

Radar absorbers are built in various forms, ranging from a thin absorber layer (paint coating) to thick pyramidal structures. Paint-coated absorbers [1] are constructed by coating the object with a lossy material so that EM energy is absorbed in a spe-

* Corresponding author: V. P. Inbavalli (inbavalli@gmail.com).

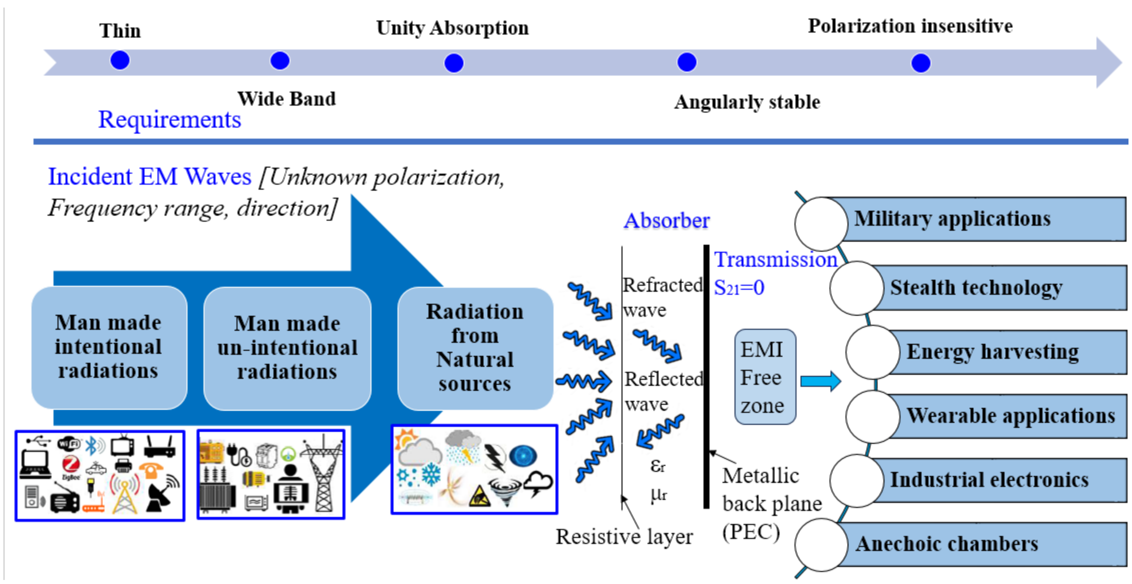

FIGURE 1. Illustration of the challenges involved in absorber design.

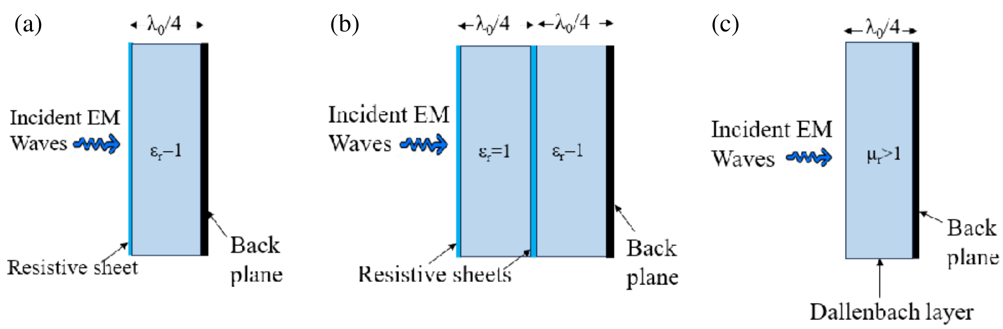

FIGURE 2. Absorber construction: (a) Salisbury screen absorber, (b) multilayer Jaumann absorber, and (c) Dallenbach absorber.

cific frequency range. The coatings get scratched or spoiled, leading to reduced lifespan and deteriorated absorbing properties, making this paint-based absorber unsuitable for stealth applications. Radar absorbers are classified under various categories based on the material properties, impedance transition, resonance conditions, and construction.

Absorbers can be classified as dielectric, magnetic, or magnetodielectric based on the materials used in construction [2]. Magnetic absorbers constructed with magnetic materials result in thin absorbers with absorption from 30 MHz to 10 GHz. Dielectric absorbers are usually thicker and work at frequencies ranging from 100 MHz to 20 GHz. Magneto-dielectric absorbers are thinner and constructed with magnetic and dielectric elements to provide the widest absorption bandwidth from 30 MHz to 20 GHz.

Based on impedance transition, absorbers are classified as (i) pyramidal, (ii) tapered load, and (iii) matching layer absorbers. Pyramidal absorbers [3] are constructed using pyramid- or wedge-shaped structures that extend in a direction normal to the assembly and are loaded with lossy elements, offering a gradual impedance transition, which finds its application in anechoic chambers. The bulky, thick, brittle nature of these absorbers makes them unsuitable for many applications. Tapering-load absorbers [4] are constructed with homogeneous resistive layers whose loading impedance increases along the propagation direction or by dispersing a homogeneous lossy material into a low-loss material parallel to the structure and with an increasing gradient in the direction of propagation. These absorbers are thinner but have poor absorption compared to the pyramidal structure. In matching layer absorbers, the impedance of the preceding layer gets transferred to the succeeding layer and added together, and finally, the impedance of the absorbing structure matches that of free space to offer absorption.

When the thickness of the absorber structure equals $\lambda_0/4$, free-space impedance matching is attained. In quarter-wavelength-based absorbers, the absorbing structures are designed with a thickness of $\lambda_0/4$. Based on quarter-wavelength resonance, absorbers are classified as (i) Salisbury screen, (ii) Jaumann, and (iii) Dallenbach absorbers. The basic Salisbury absorber [5] shown in Fig. 2(a) comprises a resistive layer located at a distance of one-fourth of a wavelength from a metallic ground plane, and the structure offers a narrow absorption bandwidth. To improve the absorption bandwidth, a multilayer Jaumann absorber [6] is constructed by employing two or more lossy layers cascaded in series, as shown in Fig. 2(b). Even though these absorbers offer an

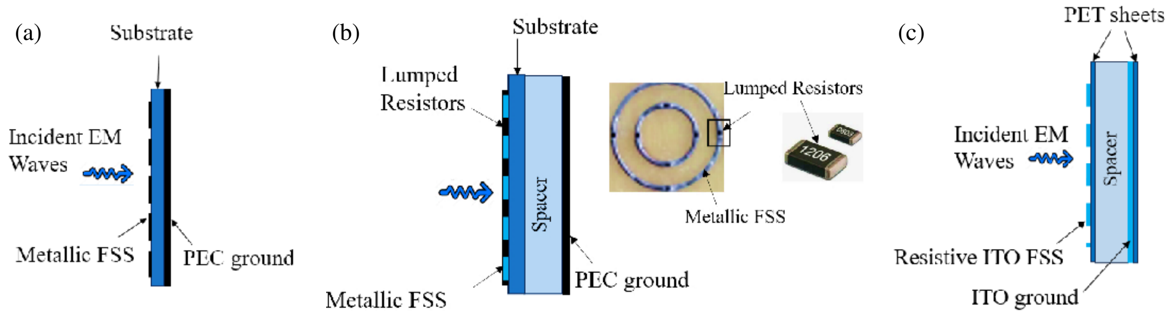

FIGURE 3. FSS-based absorber: (a) Perfect absorber, (b) Broadband absorber, and (c) Transparent absorber.

improved bandwidth, their increased thickness makes them unsuitable for practical applications. Dallenbach absorbers [7] are thin absorbers constructed by using highly lossy layers with magnetic losses and a metallic backplane, as shown in Fig. 2(c). The use of magnetic materials makes the absorber bulky and expensive. Resistive sheets are not used in these types of absorbers, and the power dissipation is caused by the lossy dielectric layer. Magnetic substances are mixed with an organic binder to form a layer of the needed loss density.

To decrease the thickness, FSS structures are incorporated in the absorber design. FSS-based absorbers are classified as perfect absorbers and broadband circuit analogue absorbers (CAA). The perfect absorbers are narrow-band absorbers, constructed with a bottom ground plane and a conducting layer consisting of periodically arranged FSS patterns at the top, with a dielectric layer in between, as shown in Fig. 3(a). The broadband CAA employs one or more lossy FSS layers in absorber design, as shown in Fig. 3(b). In this type of absorber, the incident EM wave is dissipated as ohmic loss and dielectric loss. The CAAs offer a wide bandwidth with reduced thickness. The lossy layer can be designed using a metallic FSS with lossy lumped elements, a resistive sheet, resistive ink, or carbon-based materials. These types of absorbers have a lesser profile thickness and offer broadband, angularly stable, polarization-insensitive absorption. Transparent absorbers, shown in Fig. 3(c), are designed for scenarios where optical transparency is needed for designing see-through windows and curved surfaces in stealth applications. Tunable absorbers are designed to attain impedance matching over dynamically changing EM conditions by tuning the resonance frequency and absorption bandwidth. The literature of the above-listed absorbers is reviewed in detail in succeeding sections.

2. CONVENTIONAL ABSORBERS

Conventional EM absorbers, including Salisbury and Jaumann absorbers, are the primitive form of absorbers, which work on the principle of impedance matching of resistive layers, and this is achieved by quarter-wavelength spacing from the back plane. These absorbers are usually very simple to design and offer predictable performance at desired frequencies. Their dependency on fixed spacer geometry and material properties results in relatively large physical thicknesses and fixed operational bandwidths. These absorbers are typically bulky and optimized for specific frequency bands and incidence conditions. Due to these constraints, their application is limited in recent EM radar absorption systems.

2.1. Salisbury Absorber

The Salisbury screen absorber shown in Fig. 2(a) is the simplest form of absorber with a narrow absorbing bandwidth. It consists of a thin resistive screen with impedance equal to free space (377 Ω) placed at a distance d equal to $\lambda/4$ in front of a PEC ground plane, usually separated by an air-gap spacer, first proposed by W. W. Salisbury [5]. The resistive screen is placed at a quarter-wavelength distance so that the wave travelling ahead of the resistive screen travels half a wavelength distance and undergoes a phase shift of 180°. The incident wave cancels the wave reflecting from the surface of the resistive sheet, thus nullifying the reflected wave. The spacer thickness can be reduced by replacing the air gap with a material of high permittivity at the cost of reduced bandwidth. As these absorbers show a narrow band around the resonant frequency and require a thickness of $\lambda/4$, they are not widely used in most applications. The equivalent circuit (EC) of the Salisbury screen consists of a short-circuited $\lambda/4$ transmission line.

A lot of work has been done on the Salisbury screen to improve its bandwidth. In [8], the resistive sheet in the conventional Salisbury screen is replaced by a resistive strip grating, and the ground plane is replaced by a parallel conducting grating, and an absorber has been designed for 10 GHz. This design achieves -45.2 dB return loss and -0.23 dB insertion loss for TE mode and TM mode, respectively. The design's shortcoming is that it remains transparent for TM polarization. Analytical expressions are proposed in [9] for the sheet resistance to yield the maximum bandwidth for a specified reflectivity level, incidence angle, and polarization. In [10], an optimized high-permittivity skin layer is placed above the resistive layer to improve the absorption (-20 dB bandwidth from 3 to 9 GHz) at normal incidence. In addition, the skin layer offers protection against mechanical or environmental damage. The absorber's overall thickness is 9.1 mm, and the thickness of the skin layer is 1 mm. In [11], square Salisbury screens with thicknesses between 0.5 and 7.5λ are analyzed for edge scattering using the method of moments (MoM) technique by optimizing resistivity and spacer thickness. In [12], a chip resistor grid network on cloth of thickness 0.075 mm is designed for absorption at S, C, and X bands. In [13], analytical expressions for optimum in-

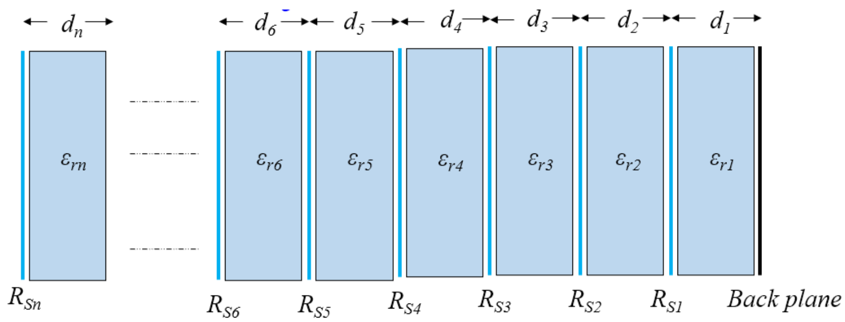

FIGURE 4. Physical topology of Jaumann absorber

ductance are calculated using a non-Foster matching technique, and the reflectivity of the Salisbury screen at oblique incidence is calculated. Negative inductance is employed in the analysis to provide broadband matching. In [14], a V-shaped absorber is developed by modifying the conventional Salisbury screen. The PEC ground is inclined to 45°, and the resistive sheet is placed vertically, providing uneven spacing between the PEC ground and resistive sheet. In [15], a 9 mm-thick polarization-insensitive, wide-bandwidth (3.74–18.5 GHz) Salisbury absorber is developed, where the metallic ground plate is substituted by the reflective square patch.

Due to the narrow bandwidth limitation of the Salisbury screen absorber, it cannot be used in a wide range of applications which demands a broad operational band. The key solution to increase bandwidth is to increase the number of resonant frequencies, and this can be done by increasing the number of layers.

2.2. Jaumann Absorbers

Jaumann absorbers are constructed by placing more than one layer of resistive sheet separated by dielectric spacers, with the highest resistance on the incidence side and the lowest resistance at the backplane to overcome the bandwidth limitation of the Salisbury absorber. This technique increases the absorber's bandwidth. Fig. 4 shows a typical n-layer Jaumann absorber. In [16], the performance of Jaumann absorbers, when they are used in cylindrical structures, has been evaluated by modifying Richmond's cylindrical stepping theory. A five-layer design has been designed with the diameter of the composite structure nearly triple that of the conducting cylinder, and the results suggest that Jaumann absorbers should not be considered for cylinders less than a wavelength in diameter. In [17], analytical formulas have been developed for multiple electric/magnetic Salisbury screens for the planar and cylindrical surfaces of two- and three-screen planar stackups.

In [6], a synthesis procedure is presented for designing absorbers with layers up to 20. An equiripple solution is described for a given number of layers and specified maximum reflection coefficient,showing a wider bandwidth than the corresponding maximally flat solution. In [18], a Chebyshev-like iterative approach is used to find unknown sheet resistivities that will minimize reflection for a given frequency bandwidth. In [19], numerical optimization based on the genetic algorithm (GA) is used to design multilayer Jaumann absorbers with optimum oblique angle performance for TE and TM modes. Three- and four-layer Jaumann absorbers are designed, and the performance is analyzed for 45° and 60°, respectively. In [20], synthesis algorithms based on Butterworth, equiripple, and Chebyshev absorption properties are used to calculate the absorber's sheet resistance with optimal bandwidth response. The results for normal incidence are given in lookup tables to assist in the design of practical Jaumann absorbers. An adaptive GA using adaptive mutation for fast convergence with a minimum profile is proposed in [21], considering one dielectric material for the spacers. A five-layer Jaumann absorber is developed, and the algorithm successfully reduces the absorber thickness by at least 45% compared to the conventional absorber. In [22], a lookup table for the design of a Jaumann absorber showing the resistive sheet values to achieve a wider bandwidth is proposed. These tables also help calculate specific narrow-bandwidth absorbers. Instead of using design formulae or lookup table, the resistance value of the multilayer resistive sheet is calculated using the Smith chart in [23, 24], allowing designers to visualize how the design achieves the desired bandwidth.

In [25], the reflection characteristics of the multilayer absorber are analyzed using the transmission line model. The Smith chart is used to analyze the effects of sheet resistance on reflection performance, and it is found that the number of layers in the design corresponds to the number of nulls in the reflection curve. In [26], either or both front and back faces of the panel of the Salisbury screen and Jaumann absorbers are inclined with respect to the incident radar signal. Here, a quasi-optical technique is used to predict the scattering parameters, since electrically large panels are considered. In [27], a numerical study is performed to find the bandwidth-to-thickness ratio of the radar absorber as a function of reflectivity for suppressing waves incident normally. Single- and multi-layer dielectric absorbers are studied, and a simple empirical relationship among thickness, bandwidth, and reflectance level is derived. In [28], a knowledge-based selection of a GA objective function to increase the absorber's bandwidth without increasing thickness at oblique angles of incidence is proposed.

In Jaumann absorbers, by increasing the number of layers, a better bandwidth can be achieved, but the thickness and weight of the absorber structure will also gradually increase, which makes it unsuitable for practical applications. To make absorbers best suited for practical applications, the absorbers should afford high bandwidth with a thin, lightweight structure. An innovative design approach is required for designing absorber structures with a lower number of layers. This paved the way for the design of FSS-based absorbers, which afford broadband absorption with thinner absorbers.

3. FSS-BASED ABSORBERS

FSS-based absorbers consist of a two-dimensional array of conductive patterns on a dielectric layer supported by a ground plane. These absorbers offer broad absorption bandwidth with comparatively less thickness than Salisbury and Jaumann absorbers. An FSS is a thin, repetitive, periodic arrangement of metallic arrays, either patches or apertures on a dielectric surface, which are designed to reflect or transmit EM fields depending on the field frequency [29, 30]. As FSS has both resistive and reactive properties, impedance matching is attained for a larger bandwidth, resulting in wider absorption with a thinner profile. These FSS-based absorbers aim at generating multiple resonances in the frequency range, reducing the overall thickness, offering a broader bandwidth, polarization insensitivity, and an angularly stable response.

Extensive research has been conducted on FSS structures employing elements of different sizes and shapes. The absorbers can be classified as narrow-band perfect absorbers or broadband CAA. The narrow-band absorbers make use of resonating metallic structures, and the broadband absorbers consist of non-resonating lossy structures.

3.1. Narrow-Band FSS Absorber

"The electrically thin profile absorbers offer near-unity absorption at a desired frequency for normal incidence and are termed perfect absorbers" [31]. These absorbers consist of metallic FSS on the top and a homogeneous metallic ground plane at the bottom. The absorber's resonant frequency is governed by the geometry of the FSS periodic elements. The substrate's dielectric properties and absorber thickness determine the resonating frequency. At the resonant frequency, the incident EM wave energy is dissipated as ohmic and dielectric losses in the metallic FSS and substrate, respectively. Combined electric and magnetic effects enable the absorber impedance to match the impedance of free space, reducing reflection, resulting in near-perfect absorption.

Research works were carried out on various shapes of resonating elements, from simple square/circular patches and square/circular/octagonal rings to advanced shapes like split-ring resonators (SRRs), cross/Jerusalem cross (JC) structures, meandered and fractal geometries, etc. Perfect absorbers guarantee absorption levels greater than 95% for normal incidence and a better angular stability, determined by the periodicity and symmetry of the unit cell. The low-profile thickness of these absorbers makes them suitable for conformal applications.

The first metamaterial absorber is proposed in [31], with the absorption of 96% at 11.5 GHz. In [32], a 3.2 mm thick absorber with Minkowski fractal geometry is proposed for multipath mitigation. The absorber offers 98% absorption at 0.868 GHz for incidence angles up to 45° and 60° for TE and TM polarizations, respectively. In [33], a high Q-factor (69.8) 0.127 mm metamaterial absorber is designed with an inverted-cross-star metal patch to resonate at 12.5 GHz. The design offers 85% absorption with angular stability of 70° [34] investigated a narrowband perfect absorber based on an InSb cylinder structure array for 99.9% absorption at 1.9 THz with a 120.9 Q-factor. In [35], a circularly polarized four-element array and a wall of the double-layer slotted cross patch metamaterial absorber are proposed to reduce mutual coupling between antennas in the array operating in 1.24–1.28 GHz. In [36], an optimal approach is used in the SRR design, which improves the signal-to-noise ratio (SNR) from 3.39 to 28.59 dB. In THz[4], GA is developed to optimize the absorption bandwidth by retrieving the physical dimensions and effective ε_r and μ_r of an absorber with periodic metallic strips for a 9 GHz center frequency. In [37], an absorber with square patch arrays on a perforated dielectric slab for metallic vias between FSS and ground is designed for perfect absorption at 3.5 GHz. This enhances the TM absorption bandwidth and absorption performance but has no effect on the TE polarization.

Due to the near-unity single-frequency absorption, applications are limited, and henceforth, to obtain multiple resonant frequencies, different resonating structures are included either horizontally or vertically to create multiple resonating structures. In [38], a triple-band absorber with a thickness of $\lambda/153$ is designed on a polyethylene terephthalate (PET) substrate, offering resonances at 6.16, 9.22, and 11.6 GHz with absorptivities of 95, 96, and 97%, respectively. In [39], a modified segmented SRR absorber is fabricated with four resonances at 11.23, 14.18, 17.37, and 19.18 GHz with absorption of 85.51, 99.13, 98.19, and 90.8%, respectively. In [40], an absorber is realized by interlaced I and square metallic stripes to produce four resonances at 2.24, 2.8, 4.3, and 5.8 GHz with absorptivities of 96, 93, 93, and 95%, respectively, and the design attains a negative ε_r and μ_r. In [41], the unit cell is replicated along the ring lattices to obtain the dual-ring three-layer absorber.

In [42], a dual-side, deca-band, FSS absorber based on surface plasmonic resonances is designed for X- to K-band applications with a thickness of $0.07\lambda_L$, offering an absorption of 94.6%. In [43], the FDTD method is used to design an absorber with four absorption peaks derived from the 3rd to 6th resonance mode couplings in the near-infrared band using a Fabry-Perot structure to offer the narrowest absorption bandwidth of 24 nm with a Q-factor of 37.6. Consequently, when a wider absorption bandwidth is required, multi-resonant structures can be designed to resonate at nearby frequencies to offer wide absorption bandwidth. In [44], an absorber with a thickness of 0.07λ is designed by realizing a periodic structure of SRR for providing 90% absorption from 8.3 to 11.3 GHz. In [45], dual-band absorbers are designed with a layer of 2 symmetrical metallic resonators (circle, square, hexagon, JC) to resonate at 2.4 and 5 GHz by using a lossy dielectric layer, and air medium is used as a spacer. In [46], an absorber consisting of a pair of co-centered resonating JCs printed on an FR4 substrate cascaded with a high-loss, dielectric layer and a metallic back plane for absorption from 7.8 to 12 GHz with a fractional bandwidth of 42.42%. Table 1 shows a comparison of narrow-band absorbers reported in the literature.

TABLE 1. Comparison of metallic FSS-based radar absorbers.

Ref.	Layer	Unit cell	No. of Freq. band	Absorption Freq. (GHz)	Angular Stability		Absorption %	Substrate	thick (mm)
					TE°	TM°			
[44]	1	SRR	1	8.3–11.3	0	0	90	FR4	4.5
[45]	2	circular ring	2	2.4, 5.15–5.89	30	30	90	FR4, Eccosorb	9
[46]	1	JC	1	7.8–12	40	60	90	FR4, Eccosorb	4.1
[47]	1	square ring	1	6.14	80	80	98	FR4	1
[48]	1	JC	5	8.8, 9, 9.3, 9.4, 10	60	60	97, 97, 96, 99, 97	FR4	2.4
[49]	1	square patch	1	0.85	0	0	98	Card board	6.5
[50]	1	petal	2	16.6, 24.4	70	70	80, 95	FR4	0.47
[51]	1	SRR	3	2.4, 5.2, 5.8	40	40	99, 98, 98	F4B	3
[52]	1	Octa ring, cross	2	12.2, 15.5	90	30	99, 90	FR4	0.75
[53]	1	bow-tie dipole	1	2.45	0	0	96	RO 4003C	8
[54]	1	SR + E-fractal	6	21.1, 22.2, 23.4, 24.9, 27.9, 29	20	20	98, 94, 97, 97, 95, 96	FR4	1.6
[55]	2	rectangle patch	2	11.3–13.5	30	30	90	FR4	4

These absorbers are employed in stealth enhancement against monostatic radar systems [42, 46, 41], mitigate scan blindness and pattern distortion in phased arrays [32], sensing applications [33, 34, 43], electromagnetic compatibility (EMC) and electromagnetic interference (EMI) suppression [36, 39, 44], antenna performance enhancement [35], and EM energy harvesting [39, 51]. The unity absorption, single-frequency resonant absorbers are very sensitive to incidence angle, polarization, parameter variations, and fabrication tolerances.

The single-frequency absorption at the resonant frequency results in high surface current and localized heating effects, limiting power-handling capability. In a practical EM scenario, maintaining strict resonance conditions is difficult. The limitations of perfect absorbers can be resolved by including resistors introduce ohmic loss into the resonant structure, which will be reviewed in the next section.

3.2. Absorbers with Metallic FSS with Lumped Resistors

These absorbers are constructed with metallic FSS loaded with lumped or distributed resistors on a dielectric substrate backed by a metallic ground plane. The geometry of the FSS layer provides capacitive and inductive resonance, and the resistors offer ohmic loss and dissipate incident EM energy into heat. When the impedance of the absorber (combined electric and magnetic resonance) matches with the fre-space impedance, an absorption band is obtained. The values of the lumped resistor, gap width, metal trace length, substrate thickness, and unit cell size control absorption level & bandwidth, capacitance, inductance, magnetic coupling, and operating frequency, respectively. Research outcomes were reported on various shapes of resonating elements loaded with lumped resistors, from simple square/circular patches and square/circular/octagonal rings to advanced shapes, such as SRR, cross, JC structure, and meandered fractal geometry.

In [56], a single-layer absorber for 10 dB reflection reduction from 1.77 to 4.33 GHz is built with bow ties of different sizes loaded with lumped resistors. A single-layer absorber with a thickness of $0.077\lambda_L$ comprising a cross dipole with lumped resistors and a central resonant patch is designed in [57] to offer an absorption bandwidth of 108.67% from 3.58 to 12.10 GHz. In [58], a single-layer $0.08\lambda_L$-thick absorber with 3 resonant modes is realized to offer a fractional bandwidth (FBW) of 127.9% from 2.68 to 12.19 GHz. In [59–70], absorbers are designed using multi-resonant phenomena with square conducting loops loaded with lumped resistors to offer absorption in a wide absorption bandwidth. In [62], a layer of dielectric skin is included in the design for an increased resonance. In [59, 65, 66], GA-based optimization is used to obtain the optimized parameters. In [68], periodic structures are printed on both sides of the substrate to improve design freedom for optimal performance. In [69, 70], a double fractal square loop structure is used to reduce the size of the unit cell for better angular stability.

In [71], a $0.32\lambda_L$ thick absorber is designed with a pair of rectangular patches and a loop loaded with resistors, which offers absorption from 5.44 to 10.21 GHz, offering a stable response for both TE and TM polarizations up to 75°. In [72], an absorber with a double-circular-loop array with lumped resistors is designed for absorption from 2 to 8.3 GHz for incident angle variations up to 40° and analyzed with ECM and Marcuvitz theory. In [73], a $0.101\lambda_L$-thick 2-layer absorber with meander lines and lumped resistors is printed on a perforated substrate to offer a bandwidth ratio of $1 : 12.88$. The perforated substrate and the air space in between are used to increase the bandwidth. With an optimum air-spacer thickness, the ab-

TABLE 2. Comparison of metallic FSS with lumped resistor radar absorbers.

Ref.	layer	Unit cell	Bandwidth		Absorption		Substrate	Thick (mm)
			f_L	f_H	TE°	TM°		
[56]	1	bow tie	1.77	4.33	0	0	Taconic	12.7
[57]	1	dipole, square patch	3.63	9.91	30	30	FR4	6.2
[58]	1	metallic strips	2.77	12.2	30	30	FR4	9
[59]	2	square loop	4.2	14	45	45	$\varepsilon_r = 1.7, 2.5$	11.5
[61]	1	DSL	2.2	9	30	30	2.2	14.2
[62]	2	square loop	2	17.1	40	40	RT5880	15.0
[63]	1	square loop	8	18	0	0	RT5880	10
[64]	2	square loop	4.96	18.2	0		FR4	4.6
[65]	2	square loop	3	8.32	45	45	2.65	10
[67]	2	square loop	1.3	10	30	30	FR4	21
[68]	2	square loop	2.22	11.5	15	15	RO 4003	10.5
[69]	2	fractal square loop	1.98	8.64	30	30	FR4	13.6
[70]	1	Minkowski fractal loops	5.5	17.5	30	0	$\varepsilon_r = 2.25$	4.5
[71]	1	square loop	5.44	10.2	75	75	3	17.5
[72]	1	circular loop	2	8.3	40	40	FR4	14.7
[73]	2	meander lines	1.03	13.3	30	30	FR4	29.6
[74]	2	circular sector	3.87	14.8	0	0	FR4	6.2
[75]	1	crossed dipole	5.3	11.2	30	60	FR4	4.47

sorption bandwidth is increased. In [74], a 2-layer absorber is constructed by a periodic pattern of circular sectors with inserted lumped resistors for absorptivity in the frequency range between 3.87 and 14.84 GHz.

In [75], a 4.47 mm-thick absorber is designed using a synthesis technique to reduce the RCS using an array of metallic crossed dipoles with resistor elements to offer a reflection reduction bandwidth of 70.7% from 5.3 to 11.2 GHz. In [76], an absorber is designed with a periodic array of microstrip lines loaded with lumped circuit elements using the singular integral equation method. In [77], a method for finding the optimality ratio of planar absorbers is proposed, and the thickness and bandwidth of absorbers are evaluated and compared with the possible optimum thickness. In [78], a single-layer absorber is designed for absorption from 6.39 to 10.7 GHz, with an anchor and hat-shaped arm ring resonator with inserted load resistors. In [79], a $0.1\lambda_L$-thick absorber is designed with lumped resistor-loaded circular-loop arrays on an FR4 substrate to offer reflectivity reduction in the frequency band 3.6–24.6 GHz. In [80], a GA-based EC design approach is used to find the absorber's optimized parameters, with operating frequency bands and total thickness as inputs for designing single- and multi-layer absorbers, with FBWs of 126 and 161%, respectively. Table 2 shows a comparison of metallic FSS with lumped resistor absorbers reported in the literature.

Although these absorbers can be used in broadband applications, the following limitations prevent practical use. The lumped resistors soldered with the FSS increase the cost and fabrication complexity for large-area absorbers. Dissimilarities in soldering joints result in uneven distribution of surface resistance, leading to variation in the absorber's performance . Parasitic inductance and capacitance introduced in the solder joints at higher frequencies changes the resonant frequency, which results in the performance degradation of the absorber. Moreover, these joints suffer from mechanical reliability issues and reduced long-term stability. To overcome these limitations, alternative approaches, such as thin-film resistive layers and printed resistive inks, offer uniformity in resistance.

3.3. Resistive Screen-Based Absorbers

Resistive screen-based absorbers are thin EM absorbers that employ a patterned lossy screen to dissipate incident EM energy. When the absorber's impedance matches the free-space impedance, reflection is minimized, and absorption is attained. These resistive screen-based absorbers are further classified based on fabrication technique: resistive film, conductive ink, and transparent conductive oxide.

3.3.1. Resistive Film-Based Absorbers

In [81], a Salisbury is designed for 8–12 GHz with the PEC ground replaced by a square patch artificial magnetic conductor (AMC) and a 400 Ω/ resistive sheet to offer reduced sensitivity up to incidence angles of 40°. In [82], a three-layer capacitive circuit absorber is designed with a bandwidth of 4–24 GHz and a total thickness of 15.1 mm, with a 28% reduction in thickness and a 57% increase in bandwidth in comparison to the Salisbury screen. In this design, at low frequencies, the band-stop resonating FSS are replaced with low-pass capacitive ones, which can be synthesized by resistive square patches, and it is shown

TABLE 3. Comparison of resistive film-based radar absorbers.

Ref.	Layer	Unit cell	Bandwidth (GHz)		Absorption		Substrate	Thick (mm)
			f_L	f_H	TE°	TM°		
[81]	1	square patch	8	12	40	40	foam	10
[82]	3	square patch	4	24	0	0	foam	15.1
[83]	3	triangle lattice	2.5	8.5	45	45		11.5
[84]	1	dipole	5.4	18	40	40	TLY-5	9
[85]	8	square patch	3.3	34.6	0	0	foam	14.5
[86]	1	square patch	11	29	30	30	foam	2
[90]	1	square patch	8.2	12.4	0	0	Glass fiber	2.93
[92]	1	hexagonal loop	7.8	24	45	45	TLY-5	3
[93]	1	square patch	9.4	17	30	0	FR4	3.3
[94]	1	square patch	7.5	13.5	0	0	RO4003	3.5
[98]	3	square patch	4	50.9	60	60	PMI foam	7.4

that higher frequencies are not influenced by these modifications. In [83], an ultra-wideband 3-layer absorber using square-patch FSS as resistive sheets and high-permittivity spacers is designed for angular stability up to 45°, offering a bandwidth of 26 GHz. In [84], a high impedance surface (HIS)-based single-layer absorber, in which two unequal-length printed dipole FSS with resistive elements sandwiched between the resistive sheet and metallic backplane with a total thickness of 9 mm, is designed to enhance the absorption bandwidth from 5.4 to 18 GHz and angular stability for incidence angles up to 40°.

In [85], an absorber with a bandwidth of 3.26–34.65 GHz and a thickness of 14.5 mm, which is only 0.7% thicker than that of the theoretical limit proposed by Rozanov, is designed. The unequal periods of the square-patch FSS make EM analysis difficult, which can be simplified by using the EC model. In [86], a multiple resonant wideband absorber is designed with a single-layer treble-square loop resistive FSS to offer a bandwidth of 10.7–29 GHz with a thickness of 2 mm. In [87], a 3-layer 12 mm-thick absorber is designed, integrating a convoluted ring and a cross formed by sputtering ITO (indium tin oxide) onto a PET substrate and Teflon layers as the spacer. The absorber offers more than 90% absorption rate in the frequency range of 2.79–20.62 GHz. In [88], a 3-layer absorber is designed with a thickness of 10 mm for a bandwidth of 3.7–11.9 GHz. In [89], a 16.8 mm-thick absorber with a hexagonal resistive patch FSS for the 1.7 to 25 GHz band is developed. The four resistive FSS layers are designed as electrically very thin printed circuit boards (PCBs) using a 0.2 mm-thick FR4 substrate by accurate photolithographic technology. In [90], an absorber in the X-band is designed with a resistive square FSS and a carbon fabric composite, which is applied to the leading edge of a wing-shaped structure. The synthesis procedure for low-profile frequency-selective EM absorbers with well-defined absorption and reflection bands as well as steep selectivity is detailed in [91]. A 2nd-order absorber has been fabricated using non-resonant sub-wavelength resistive patches with a thickness of 8.9 mm, with absorption from 8.7 to 11.6 GHz.

In [92], a 3 mm-thick four-resistively-loaded hexagonal-loop FSS absorber, which exhibits absorption from 7.8 to 24 GHz, is designed by merging reflection nulls created by the 4 loops. In [93], a single-layer absorber with a square-patch FSS is designed for 9.4–17 GHz, which is constructed by placing a resistive square patch on an FR4 substrate attached using adhesive. In [94], a 3.5 mm-thick CAA with a resistive square-patch FSS is designed to have absorption in 7.5–13.5 GHz, using the synthesis formula. In [95], a multiband resistive absorber was constructed using a 2-layer cross dipole FSS for absorption at 4.9–7.3, 8.5–9.6, and 11.7–13.9 GHz. A 12 mm PET ITO resistive absorber with a JC unit cell is developed using a target-driven inverse design by deep learning in [96] with a test accuracy of 93.5%. In [97], a $0.117\lambda_L$ thick absorber is designed for absorption from 0.2 to 1.1 GHz, based on the concept of a tightly coupled array and antenna reciprocity theory using a patterned ITO. In [98], a multilayer absorber is designed using polymethacrylimide (PMI) foams and square patches of ITO resistive film FSS to offer absorption from 4 to 50.9 GHz. The absorber uses two dielectric matching layers, an equivalent media layer with an ε_r of 1.5, and PEEK (polyether ether ketone) material with an ε_r of 3.2 to enhance the absorbing stability at oblique incidences. Table 3 shows a comparison of resistive film-based absorbers reported in the literature.

3.3.2. Screen Printed Absorbers

In these absorbers, resistive layers (homogeneous/patterned) are deposited by screen-printing onto dielectric substrates with printable conductive or resistive inks, made of carbon, graphite, graphene, or metal-polymer composites. In this process, the ink is forced through a patterned mesh screen onto the substrate using a squeegee, and the printed geometry is defined by the screen's open areas and then cured at moderate temperatures. Due to the ease of bulk production and low fabrication cost, screen-printed absorbers are designed for RCS reduction and EMI/EMC mitigation.

In [99], a 1 mm-thick absorber consisting of a square-ring array printed with resistive ink on a thin grounded dielectric slab to offer absorption in 7–20 GHz. In [100], an $0.076\lambda_L$-thick absorber is realized by patterning the carbon ink as a square loop

TABLE 4. Comparison of screen-printed radar absorbers.

Ref.	Layer	Unit cell	Ink	Band width		Absorption		Substrate	Thick (mm)
				f_L	f_H	TE°	TM°		
[23]	4	square ring	conductive	8	12.2	15	30	FRP, PI	14.6
[99]	1	square ring	resistive	7	20	30	30	FR4	2
[100]	1	square loop	carbon	8	12	45	30	E-glass	3.4
[101]	3	cross, square ring	carbon	2	23	45	45	pet on PMI	3.3
[103]	1	circular ring	carbon	8	20.1	45	45	paper	15.4
[104]	4	cross, square patch	resistive	2	37.5	30	45	FR4	3.7
[105]	1	Modified JC	silver	8	10.9	0	0	PET	
[106]	1	cross, circular ring	carbon	4	12	60	60	PI, glass	25.3

on glass fabric/epoxy laminate with grounded Cu foil, showing absorption in the X-band. In [101], a 3-layer $0.1\lambda_L$-thick absorber is designed using resistive periodic square patches, square loops, and cross layers printed on a PET substrate using an inkjet printer with PMI spacers to offer absorption from 2 to 23 GHz. In [102], a $0.108\lambda_L$-thick resistive ink-based multilayer absorber is printed on an FR4 substrate for absorption in the 1.3–18.6 GHz band. In [103], a 3.36 mm-thick conformal absorber is designed, including a resistive ring-shaped FSS printed with carbon-based paint on a flexible photo paper substrate for absorption from 8 to 20.12 GHz. In [104], a four-layer resistive ink-based absorber is presented for absorption in 2.1 to 37.5 GHz, utilizing a space mapping algorithm to optimize the reflection coefficient in the degraded frequency band. A flexible CAA is realized in [105] using a screen-printing technique for absorption in the 8.3–10.9 GHz band. In [106], an absorber is designed using a GA-based algorithm and screen-printed with carbon ink on a polyimide (PI) film with a foam spacer, for RCS reduction of curved aircraft wing structures of UAVs with a curvature of 200 mm employing a pixelated metasurface for absorption in the C and X bands. In [107], the characteristics of CAAs due to manufacturing uncertainty and fabrication errors are examined by considering randomly fabricated samples designed for the X band with a square loop printed with non-uniform thickness of conductive inks on a PI film substrate where the sample is sandwiched by fiber-reinforced plastic on both sides.

Table 4 shows a comparison of screen-printed absorbers reported in the literature is. The limitations of screen-printed resistive-ink absorbers include limited printing resolution, non-uniform sheet resistance, poor electrical stability over time, and mechanical degradation under bending.

4. THREE-DIMENSIONAL (3D) ABSORBERS

A new type of absorbing structure referred to as a 3D EM absorber uses volumetric field interaction instead of just planar surface resonance to achieve EM attenuation. Unlike conventional two-dimensional absorbers, 3D absorbers exploit thickness, geometry, and material gradients to enhance EM loss, enabling broadband, wide-angle, and polarization-insensitive absorption.

In [108], hexachiral honeycomb dielectric slabs are used to increase the mechanical and EM performance. Salisbury and Jaumann absorbers are designed with hexachiral honeycomb dielectrics for frequencies of 1.5 GHz and 0.5–2 GHz, respectively. In [109], a GA-optimized absorber is designed using a patterned resistive sheet placed in a planar direction with a 2 mm-thick substrate and metallic line arrays with a 0.4 mm-thick substrate placed vertically to offer absorption from 8.2 to 19.5 GHz. In [110], a 3D absorber is realized with two lossy layers constructed by metallic strips and resistors with a double-sided parallel-strip line printed along the longitudinal direction to offer absorption from 1.50 to 12.31 GHz. In [111], a 13 mm thick absorber consisting of a planar array of resistance-loaded metallic cross patterns and a vertical crossed mesh array with resistance-loaded metallic ring patterns is realized to offer absorption between 2.11 and 3.89 GHz. A 3D absorber is designed in [112], consisting of a vertical absorbing layer with 2 elliptical resistive rings and the horizontal metallic meandered JC. Vertical and horizontal layers offer absorption from 12 to 18 GHz. A spoof surface plasmon polariton-based absorber proposed in [113] consists of 9 incurved metallic strips loaded with lumped resistors to offer absorption from 6.95 to 17.54 GHz.

In [114], a 10 mm-thick pyramidal honeycomb absorber is printed using carbon-loaded polylactic acid, with the 3D printing technique, offering an absorption level greater than 22.9 dB for a bandwidth of 2–18 GHz. In [115], a 3D absorber using carbon-doped conductive silicone rubber composite material based on a hauberk structure is designed to offer 80% absorption from 10 to 40 GHz. In [116], a two-layer 3D absorber is designed for absorption from 5.9 to 19.17 GHz with a resistive paint applied uniformly in the shape of strips on a Polylactic Acid (PLA) Swiss cross-shaped substrate.

3D EM absorbing structures suffer from challenges, such as fabrication complexity, size, weight, and integration with linear platforms. Ongoing research aims at addressing these issues through lightweight materials, structural optimization, and reconfigurable volumetric designs. As fabrication technologies emerge, 3D EM absorbers will play a significant part in forthcoming wide-band, flexible, and adaptive EM absorption systems.

TABLE 5. Comparison of transparent radar absorbers.

Ref.	Layer	Unit cell	Bandwidth (GHz)		Angular Stability		Absorptivity %	Substrate	Thick (mm)
			f_L	f_H	TE°	TM°			
[119]	1	square loop & patch	4	17.2	20	30	90	PET	5.7
[121]	1	square patch	9	17	0	0	90	PET	4
[122]	1	square silver mesh	73.5	110	45	30	90	PET	0.5
[123]	1	gear	3.86	15	15	45	90	PET, PMMA	4.5
[124]	2	cross	23.2	33.4	60	60	80	Glass	1.1
[125]	2	cross, square	2.6	19.8	0	0		PET	10
[126]	1	encapsulated water	10.45	11.2	30	30	90	PDMS	9
[127]	2	octagonal patch	5.5	24.3	60	60	90	PET, PMMA	6.5

5. TRANSPARENT ABSORBERS

Metallic or carbon-based absorbers are good at EM absorption, but they are generally opaque and hence inappropriate for applications in aircraft canopies, vehicle windshields, display panels, sensor windows, and optoelectronic enclosures where transparency is needed. To enable EM absorption without compromising the optical functionality, transparent absorbers are designed using transparent conductive oxides like ITO, graphene, and thin metallic meshes. A graphene-based transparent Salisbury absorber [117] is developed using two oppositely doped graphene sheets separated by a $\lambda/4$ lossless spacer. A highly doped graphene acts as the ground, and absorption higher than 90% is attained over a bandwidth of about 2 GHz. In [118], a partially transparent Jaumann absorber for a frequency band of 2–16 GHz is designed with a triangular lattice arrangement for an aircraft wing profile. Desired low-pass characteristics for TEz polarization and blocking TMz polarization is achieved by replacing the metallic sheet of the Jaumann by a triangular lattice FSS Gangbuster. This replacement offers a transparent window for an antenna operating at 1 GHz. In [119], an optically transparent 5.65 mm-thick absorber, based on interdigital capacitive structures, is designed with patterned ITO resistive films on PET sheets, resulting in absorption from 4 to 17.20 GHz. In [120], an ITO resistive sheet-based absorber is constructed with cross, square, and triangular patches with absorption between 16 and 27 GHz and added to a chip for EM suppression. In [121], an absorber based on temporal coupled-mode theory is realized using ITO-coated PET sheets to resonate at 12 GHz, offering reflection reduction across the X- and Ku-bands. An algorithm to involve phase response, including curvature change information, is developed. In [122], a transparent and flexible mm-wave absorber is proposed for absorption in the 73.5–110 GHz frequency band. The structure's top layer is fabricated with a silver mesh structure by the electrohydrodynamic printing technology. The transmittance of the absorber design in the visible band is 58.1%. A transparent absorber using gear wheel-shaped ITO FSS-coated PET sheets on a PMMA substrate and with a thickness of $0.218\lambda_L$ is designed in [123] to offer absorption from 3.86 GHz to 15.04 GHz. In [124], a 0.079λ-thick two-layer transparent absorber is designed for EM radiation suppression of miniaturized electronic devices using ITO resistive films in the 23.2 to 33.4 GHz spectra and perfect absorption at 28 GHz, with an absorption rate of 99.999%. The absorber is integrated onto a system-level chip with a patch antenna for EM radiation suppression up to 22 dB at a 3 m distance. In [125], a 3-layer $0.091\lambda_L$ thick optically transparent absorber is designed with a cross-square ring staggered rectangular conductive ITO FSS film to offer absorption from 2.62 to 19.81 GHz for jamming of passive microwave remote sensing using the benefits of metamaterial absorbers. In [126], a transparent absorber is realized using only dielectric materials (PDMS and water) without a conducting layer to have a maximum absorptivity at 10.8 GHz and 10.45–11.20 GHz. The water's high permittivity and high tangential loss make it suitable for absorbing EM radiation. Table 5 shows a comparison of transparent EM absorbers reported in the literature.

Significant research works have been done in the field of transparent absorbers by using transparent conductive oxides and multilayer FSS, enabling effective EM absorption without compromising the optical transparency. The fabrication limitation due to the brittle nature of the conducting oxides, which results in cracking under conformal applications, can be rectified by using ultra-thin ITO layers or by using metal nanowires, graphene, or hybrid oxide-metal-oxide stacks.

6. TUNABLE ABSORBERS

As the Salisbury, Jaumann, and FSS-based absorbers discussed in earlier sections are limited to predefined frequency bands and angular stability, they do not provide effective suppression against continuously changing agile radar signals. This challenge can be addressed by using reconfigurable and tunable absorbers that allow real-time tuning of the resonance frequency and absorption bandwidth, ensuring impedance matching under dynamically changing spectral conditions.

In [128], a theoretical phase-switched screen technique for realizing active material dynamic control of RCS at microwave frequencies (6–14 GHz) using a PIN diode-loaded bow-tie arrangement is proposed. By periodically altering the surface admittance, the reflected wave is being binary phase-modulated so that all the energy at the incident wave frequency is redistributed into sidebands. A fixed and frequency-tunable Salisbury absorber with reduced size is developed in [129] using a polymer-loaded composite sheet that possesses resistive and capacitive properties. Using a polypyrrole-loaded composite layer with sheet capacitance of 100 fF/ reduces the absorber thickness to 2 mm from 7.5 mm for $f_c = 10$ GHz absorption, at the cost of reduced bandwidth. In [130], a tunable intensity-dependent metasurface absorber for continuous surface waves is realized with PIN diode-loaded unit cells. With an increase in the power level from 5 to 20 dBm, absorption is improved from 19.4% to 92.7%, and the bandwidth is enhanced from 4.93 to 5.56 GHz. In [131], an active absorber is designed to have switching rates more than 20 MHz with an active PIN diode-loaded FSS to dynamically control the frequency range over 9 to 13 GHz. In [132], an electrically thin (0.15λ) adaptive Salisbury absorber backed with HIS ground is constructed on a 250 µm-thick liquid crystal substrate to obtain a reflectivity below -10 dB in the frequency range 8.8–10.05 GHz. The voltage-dependent anisotropic property of nematic state liquid crystals is exploited to obtain a shift in the resonant frequency of the radar absorber. In [133], a tunable absorber is designed to vary the substrate thickness using PIN diodes so that the absorption bandwidth is switched between two different frequency ranges. When the diode is ON, the bottom plate acts as a reflector, and the absorption band is from 2.08 to 4.94 GHz, and under OFF conditions, the absorption band is from 3.68 to 11.80 GHz. In [134], a tunable absorber with varactor diodes is designed where the frequency of the reflective notch is adjusted by varying the bias voltage for reflection reduction in the frequency spectrum from 2 to 8 GHz. In [135], a transparent and flexible graphene-based absorber where the graphene is patterned as periodic strip bands with a rectangular hole sandwich structure, transparent flexible PVC, and an ITO bottom plate is designed. The graphene layer is tuned to have sheet resistance of 70, 240, and 350 Ω/ to offer dual-band, wide-band, and single-band absorption spectra, respectively.

In [136], a tunable absorber is realized with a four-patch array loaded with PIN diodes. By changing the bias voltage, absorption is tuned from 8.5 to 18.2 GHz. In [137], a dual-band energy-selective surface is designed with an absorptive layer and a switchable layer for transmitting low-power signals from 3.76 to 5.86 GHz and absorbing 1.81 to 3.43 GHz and 4.1 to 5.59 GHz. In [138], a tunable CAA is realized with a double-sided FR4 substrate by printing a square patch surrounded by a split loop. Here, a PIN diode is used for tuning the 1–2.5 GHz band, and a varactor is used to tune the 0.4–1 GHz band. In [140], a tunable absorber is designed for changing the thickness electronically for two switchable operations in frequency ranges from 0.85 to 1.88 GHz and from 2.66 to 5.23 GHz by controlling the path of the RF signal using PIN diodes. In [141], a reconfigurable graphene-based absorber with a thickness of $0.06\lambda_L$ is designed by sandwiching a layer of periodically patterned graphene on PVC and placing it on the top of a metallic square patch. The bias voltage is varied for additional distributed capacitance, and the gap between patterned graphene can be altered, resulting in a dynamically tunable absorber from 13.9 to 16.4 GHz. An absorber consisting of a graphene layer and a resistive FSS layer is designed in [142]. By changing the bias voltage, the resistance of the graphene layer can be varied from 120 to 700 Ω/, resulting in a tunable absorption of 2.9 to 15.9 GHz. In [143], a graphene-based dynamically tunable absorber with a resistive layer whose surface resistance is varied from 80 to 380 Ω/ to tune the absorptivity between 80% and 50% in the frequency range from 5 to 31 GHz is designed. In [144], a reconfigurable absorber with a split annular ring patch with integrated PIN diodes is proposed with uniform control of reflectivity in the 4 to 18 GHz band by varying the bias voltage. A 2-layer absorber [145] with dual notch bands and 3 absorption bands is designed. The tunable range of the center notch frequency is from 6.88 to 7.78 GHz and 12.05 to 13.36 GHz for the lower and upper notches, respectively. In [146], a CAA is realized with lumped resistors inserted into a metallic square loop and an inner circular patch connected to the PIN diode connected feed network through metallic vias. When the diode is in the OFF state, the absorber acts as a dual-band absorber, and when the diode is in the ON state, the diode acts as a switchable radiator.

Table 6 shows a comparison of tunable EM absorbers reported in the literature. Tunable EM absorbers play a vital role in the progression to adaptive, intelligent EM absorbers capable of absorbing in a varying frequency spectral environment. By offering real-time control of the absorption frequency, bandwidth, and magnitude, they overcome the shortcomings of passive absorbers. Finally, tunable absorbers will play a vital role in the future of stealth and EMC solutions.

7. FUTURE TRENDS

Artificial intelligence, programmable metasurfaces, and multifunctional absorber architectures are emerging as important research directions in electromagnetic absorber technology. Conventional absorber design relies on repeated full-wave electromagnetic simulations and iterative optimization, which are computationally intensive. Recent advances in machine learning (ML) and deep learning (DL) have enabled rapid prediction of absorber performance, inverse design, and geometry optimization with significantly reduced computational effort. DL has been successfully employed to design thin, broadband, polarization-insensitive absorbers, while ML-based optimization techniques facilitate efficient exploration of complex metamaterial design spaces [147]. Furthermore, programmable metasurfaces employing electronically reconfigurable unit cells based on PIN diodes, varactors, MEMS switches, or integrated control circuits enable dynamic tuning of resonance frequency, bandwidth, and absorption characteristics, thereby supporting adaptive stealth and intelligent electromagnetic environments [148, 149]. In parallel, increasing attention has been directed toward multifunctional electromagnetic absorbers [150], which combine electromagnetic absorption with additional functionalities such as EM shielding, antenna integration, sensing, energy harvesting, and structural support.

Such integrated architectures [151] improve system compactness, reduce weight, and enhance platform functionality. Block-building architecture based on freestanding resistive films has been demonstrated in [152] for broadband absorption while simultaneously providing multifunctional structural capabilities. These emerging technologies are expected to play a

TABLE 6. Comparison of tunable EM absorbers.

Ref.	Layer	Bandwidth (GHz)			Absorption			Thick (mm)	Tuning mechanism
		f_L	f_H	%	TE°	TM°	%		
[134]	1	2	8	120	0	0	90	14	Varactor diode
[135]	2	8.52	17	66.3	55	55	80	3.33	Graphene
[136]	2	8.5	18.2	72.6	30	10	90	3.3	PIN Diode
[137]	2	1.86	6.3	108	0	0	80	15.5	PIN diode
[138]	1	0.4	2.5	144.8	45	45	90	25.15	Varactor diode
[139]	2	8	14	54.54	30	45	90		Plasma
[140]	1	13.9	16.4	16.5	0	0	90	1.19	Graphene
[142]	1	2.9	15.9	132	20	20	90	15	Graphene
[143]	2	5	31	144	15	15	80	6	Graphene
[144]	1	4	18	127	30	30	90	6.25	PIN diode
[145]	2	7.1	7.6	7.6	30	30	90	6	PIN Diode
		12.9	13.6	4.9					

TABLE 7. Effect of design parameters on absorber performance.

Design Parameter	Variation	Effect on Absorber Performance
Number of layers	Multiple	Wider absorption bandwidth, enhanced angular stability
Number of FSS	Multiple	Multiple resonance, broadband absorption due to interlayer EM coupling
Resistance value	Low	Higher Q-factor, narrow bandwidth
	High	Increased ohmic loss, wider absorption bandwidth
Dielectric thickness	Increase	Enhanced electric field, lower resonant frequency, increased thickness
Spacer thickness	Increase	lower resonant frequency, enhanced bandwidth, excessive thickness
Dielectric permittivity	High	Miniaturization, lower operating frequency, reduced angular stability, increased dielectric loss
	Low	Improved bandwidth, enhanced angular stability, large unit-cell size
Unit-cell size	Larger	Lower resonant frequency, grating lobes at higher frequencies
	Smaller	Higher resonant frequency, better angular stability
FSS symmetry	Symmetric	Polarization-insensitive absorption
	Asymmetric	Polarization-sensitive absorption

significant role in developing next-generation intelligent electromagnetic absorbing systems.

Absorber design involves balancing various absorber parameters such as absorption bandwidth, absorption magnitude, angular stability, thickness, and fabrication complexity. Therefore, an optimized design is required to have a balanced compromise between these parameters. Table 7 shows the effect of various design parameters on the performance of the absorber.

8. CONCLUSION

This review paper outlines the trajectory from passive absorber to intelligent tunable absorbers for their use in modern radar and communication systems. A comparison of the various absorber technologies in the proposed review article reveals that no single approach simultaneously satisfies all electromagnetic and practical design requirements. Despite simple design and low fabrication cost, the conventional Salisbury absorbers suffer from narrow bandwidth and quarter-wavelength thickness. Bandwidth improvement is achieved through multilayer Jaumann absorbers at the expense of increased thickness and weight. FSS-based absorbers achieve an optimum balance among bandwidth, low profile, angular stability, and polarization insensitivity, making them suitable for modern stealth and EMC applications. Resistive screen absorbers offer broadband performance through printed or resistive-film technologies with simple fabrication techniques. Transparent absorbers offer optical transparency in addition to electromagnetic absorption for applications that require transparency, such as aircraft canopies and sensor window at the cost of fabrication complexity and material cost. Absorption in real-time changing electromagnetic environment is enabled by tunable absorbers, but their active biasing networks increase the system complexity, power consumption, and implementation cost. Therefore, selecting an absorber technology ultimately depends on the application-specific trade-off among bandwidth, thickness, weight, fabrication complexity, transparency, adaptability, and overall system cost. Despite significant progress, achieving an optimal balance among ultra-wideband absorption, low-profile design, wide-angle stability, lightweight construction, and low fabrication complexity within a single absorber architecture remains a major challenge. Furthermore, scalable manufacturing and practical integration of intelligent reconfigurable absorbers into real-world platforms require further investigation.

REFERENCES

[1] Folgueras, L. d. C., M. A. Alves, and M. C. Rezende, "Electromagnetic radiation absorbing paints based on carbonyl iron and polyaniline," in *2009 SBMO/IEEE MTT-S International Microwave and Optoelectronics Conference (IMOC)*, 510–513, Belem, Brazil, 2009.

[2] Kalraiya, S., "Development of polarization-insensitive metamaterial absorber (RASORBER) structures for multiband and wideband applications," Ph.D. dissertation, Indian School of Mines (ISM), Dhanbad, India, 2022.

[3] DeWitt, B. T. and W. D. Burnside, "Electromagnetic scattering by pyramidal and wedge absorber," *IEEE Transactions on Antennas and Propagation*, Vol. 36, No. 7, 971–984, July 1988.

[4] Huang, R., Z.-W. Li, L. B. Kong, L. Liu, and S. Matitsine, "Analysis and design of an ultra-thin metamaterial absorber," *Progress In Electromagnetics Research B*, Vol. 14, 407–429, 2009.

[5] Salisbury, W. W., "Absorbent body of electromagnetic waves," U.S. Patent 2,599,944, June 1952.

[6] Du Toit, L. J. and J. H. Cloete, "Advances in the design of Jaumann absorbers," in *International Symposium on Antennas and Propagation Society, Merging Technologies for the 90's*, Vol. 3, 1212–1215, Dallas, TX, USA, May 1990.

[7] Chambers, B. and A. Tennant, "Active Dallenbach radar absorber," in *2006 IEEE Antennas and Propagation Society International Symposium*, 381–384, Albuquerque, NM, USA, July 2006.

[8] Gross, F. and E. Kuster, "An optimized polarization sensitive Salisbury screen," *IEEE Transactions on Antennas and Propagation*, Vol. 35, No. 12, 1492–1495, December 1987.

[9] Chambers, B., "Optimum design of a Salisbury screen radar absorber," *Electronics Letters*, Vol. 30, No. 16, 1353–1354, August 1994.

[10] Chambers, B. and A. Tennant, "Characteristics of a Salisbury screen radar absorbercovered by a dielectric skin," *Electronics Letters*, Vol. 30, No. 21, 1797–1799, October 1994.

[11] Haupt, R. L., "Scattering from small salisbury screens," *IEEE Transactions on Antennas and Propagation*, Vol. 54, No. 6, 1807–1810, June 2006.

[12] Sudhendra, C., V. Mahule, A. C. R. Pillai, and A. Mohanty, "A novel space cloth using resistor grid network for radar absorbers in stealth applications," in *2011 International Conference on Communications and Signal Processing*, 83–86, Kerala, India, February 2011.

[13] Ford, K. L., "Oblique incidence analysis of a Salisbury screen employing a non-foster matching technique," in *2013 Loughborough Antennas & Propagation Conference (LAPC)*, 510–513, Loughborough, UK, November 2013.

[14] Qiu, S., H. Yu, and Z. Li, "Design of V-shaped Salisbury screen absorber," in *2020 9th Asia-Pacific Conference on Antennas and Propagation (APCAP)*, 1–2, Xiamen, China, August 2020.

[15] Zhou, Z., K. Chen, B. Zhu, J. Zhao, Y. Feng, and Y. Li, "Ultra-wideband microwave absorption by design and optimization of metasurface Salisbury screen," *IEEE Access*, Vol. 6, 26 843–26 853, 2018.

[16] Knott, E. and K. Langseth, "Performance degradation of Jaumann absorbers due to curvature," *IEEE Transactions on Antennas and Propagation*, Vol. 28, No. 1, 137–139, January 1980.

[17] Fante, R. L. and M. T. McCormack, "Reflection properties of the Salisbury screen," *IEEE Transactions on Antennas and Propagation*, Vol. 36, No. 10, 1443–1454, 1988.

[18] Toit, du L. J. and J. H. Cloete, "Optimal equiripple solution to the Jaumann absorber problem," in *IEEE Antennas and Propagation Society International Symposium 1992 Digest*, Vol. 2, 703–706, Chicago, IL, USA, June 1992.

[19] Chambers, B. and A. Tennant, "Design of wideband Jaumann radar absorbers with optimum oblique incidence performance," *Electronics Letters*, Vol. 30, No. 18, 1530–1532, September 1994.

[20] Du Toit, L. J. and J. H. Cloete, "Electric screen Jauman absorber design algorithms," *IEEE Transactions on Microwave Theory and Techniques*, Vol. 44, No. 12, 2238–2245, December 1996.

[21] Foroozesh, A. R., A. Cheldavi, and F. Hodjat, "Design of Jaumann absorbers using adaptive genetic algorithm," in *2000 5th International Symposium on Antennas, Propagation, and EM Theory. ISAPE 2000 (IEEE Cat. No.00EX417)*, 227–230, Beijing, China, August 2000.

[22] Nortier, J. R., "Tables for the design of Jaumann microwave absorbers," *Microwave Journal*, 219–222, 1987.

[23] Neo, C. P., Y. J. Zhang, W. J. Koh, L. F. Chen, C. K. Ong, and J. Ding, "Smith chart approach to the design of multilayer resistive sheet," *IEEE Microwave and Wireless Components Letters*, Vol. 13, No. 1, 24–26, January 2003.

[24] Inbavalli, V. P., V. P. Sakthivel, C. Venkatesh, and T. R. SureshKumar, "Design and analysis of radar absorbers using smith chart," in *2022 IEEE Microwaves, Antennas, and Propagation Conference (MAPCON)*, 1509–1513, Bangalore, India, December 2022.

[25] Li, K., X. Zhang, X. Hou, and P. Zhang, "Analysis and design of multilayer Jaumann absorbers," in *2011 IEEE International Conference on Microwave Technology & Computational Electromagnetics*, 81–84, Beijing, China, May 2011.

[26] Chambers, B., "Characteristics of radar absorbers with tapered thickness," in *IEE National Conference on Antennas and Propagation*, 27–30, York, UK, March 1999.

[27] Rozanov, K. N. and S. N. Starostenko, "Numerical study of bandwidth of radar absorbers," *The European Physical Journal Applied Physics*, Vol. 8, 147–151, September 1999.

[28] Bajwa, A., T. Williams, and M. A. Stuchly, "Design of broadband radar absorbers with genetic algorithm," in *IEEE Antennas and Propagation Society International Symposium. 2001 Digest. Held in conjunction with: USNC/URSI National Radio Science Meeting (Cat. No.01CH37229)*, Vol. 4, 672–675, Boston, MA, USA, July 2001.

[29] Munk, B. A., *Frequency Selective Surfaces: Theory and Design*, Wiley, 2005.

[30] Celozzi, S., R. Araneo, and G. Lovat, *Electromagnetic Shielding*, John Wiley & Sons, 2008.

[31] Landy, N. I., S. Sajuyigbe, J. J. Mock, D. R. Smith, and W. J. Padilla, "Perfect metamaterial absorber," *Physical Review Letters*, Vol. 100, May 2008.

[32] Venneri, F., S. Costanzo, and G. D. Massa, "Fractal-shaped metamaterial absorbers for multireflections mitigation in the UHF band," *IEEE Antennas and Wireless Propagation Letters*, Vol. 17, No. 2, 255–258, February 2018.

[33] Zhu, H., Y. Zhang, L. Ye, Y. Li, Z. Dang, R. Xu, and B. Yan, "A high Q-factor metamaterial absorber and its refractive in-

dex sensing characteristics," *IEEE Transactions on Microwave Theory and Techniques*, Vol. 70, No. 12, 5383–5391, December 2022.
[34] Chen, F., Y. Cheng, and H. Luo, "Temperature tunable narrowband terahertz metasurface absorber based on InSb microcylinder arrays for enhanced sensing application," *IEEE Access*, Vol. 8, 82 981–82 988, 2020.
[35] Zhang, J., J. Li, and J. Chen, "Mutual coupling reduction of a circularly polarized four-element antenna array using metamaterial absorber for unmanned vehicles," *IEEE Access*, Vol. 7, 57 469–57 475, 2019.
[36] Yuan, J., H. An, J. Li, C. Yang, L. Cao, and T. Ye, "Decoupling analysis of structural parameters in the robust design of metamaterial absorber," *IEEE Transactions on Electromagnetic Compatibility*, Vol. 64, No. 5, 1330–1336, October 2022.
[37] Luukkonen, O., F. Costa, C. R. Simovski, A. Monorchio, and S. A. Tretyakov, "A thin electromagnetic absorber for wide incidence angles and both polarizations," *IEEE Transactions on Antennas and Propagation*, Vol. 57, No. 10, 3119–3125, October 2009.
[38] Kalraiya, S., R. K. Chaudhary, and R. K. Gangwar, "Polarization independent triple band ultrathin conformal metamaterial absorber for C-and X-frequency bands," *AEU — International Journal of Electronics and Communications*, Vol. 135, 153752, 2021.
[39] Hannan, S., M. T. Islam, N. M. Sahar, K. Mat, M. E. H. Chowdhury, and H. Rmili, "Modified-segmented split-ring based polarization and angle-insensitive multi-band metamaterial absorber for X, Ku and K band applications," *IEEE Access*, Vol. 8, 144 051–144 063, 2020.
[40] Edries, M., H. A. Mohamed, S. S. Hekal, M. A. El-Morsy, and H. A. Mansour, "A new compact quad-band metamaterial absorber using interlaced I/square resonators: Design, fabrication, and characterization," *IEEE Access*, Vol. 8, 143 723–143 733, 2020.
[41] Ren, J., S. Gong, and W. Jiang, "Low-RCS monopolar patch antenna based on a dual-ring metamaterial absorber," *IEEE Antennas and Wireless Propagation Letters*, Vol. 17, No. 1, 102–105, January 2018.
[42] Singh, A. K., M. P. Abegaonkar, and S. K. Koul, "Dual-and triple-band polarization insensitive ultrathin conformal metamaterial absorbers with wide angular stability," *IEEE Transactions on Electromagnetic Compatibility*, Vol. 61, No. 3, 878–886, June 2019.
[43] Wu, P., Y. Wang, Z. Yi, Z. Huang, Z. Xu, and P. Jiang, "A near-infrared multi-band perfect absorber based on 1D gold grating Fabry-Perot structure," *IEEE Access*, Vol. 8, 72 742–72 748, 2020.
[44] Zuo, P., T. Li, M. Wang, H. Zheng, and E.-P. Li, "Miniaturized polarization insensitive metamaterial absorber applied on EMI suppression," *IEEE Access*, Vol. 8, 6583–6590, 2020.
[45] Zhekov, S. S., P. Mei, G. F. Pedersen, and W. Fan, "Hybrid absorber with dual-band performance and high absorption rate," *IEEE Transactions on Electromagnetic Compatibility*, Vol. 65, No. 1, 79–87, February 2023.
[46] Palaniappan, I. V., S. T. Rajamanickam, S. V. Ponnuvel, and V. Chakrapani, "Bandwidth enhancement of resonating absorber using a lossy dielectric layer for RCS reduction in X-band," *Frequenz*, Vol. 79, No. 5-6, 213–219, January 2025.
[47] Ghosh, S. and K. V. Srivastava, "An equivalent circuit model of FSS-based metamaterial absorber using coupled line theory," *IEEE Antennas and Wireless Propagation Letters*, Vol. 14, 511–514, 2015.
[48] Charola, S., S. K. Patel, J. Parmar, and R. Jadeja, "Multiband Jerusalem cross-shaped angle insensitive metasurface absorber for X-band application," *Journal of Electromagnetic Waves and Applications*, Vol. 36, No. 2, 180–192, 2022.
[49] Costa, F., S. Genovesi, A. Monorchio, and G. Manara, "Low-cost metamaterial absorbers for sub-GHz wireless systems," *IEEE Antennas and Wireless Propagation Letters*, Vol. 13, 27–30, 2014.
[50] Wang, J., R. Yang, J. Tian, X. Chen, and W. Zhang, "A dual-band absorber with wide-angle and polarization insensitivity," *IEEE Antennas and Wireless Propagation Letters*, Vol. 17, No. 7, 1242–1246, July 2018.
[51] Wei, Y., J. Duan, H. Jing, Z. Lyu, J. Hao, and Z. Qu, "A multi-band, polarization-controlled metasurface absorber for electromagnetic energy harvesting and wireless power transfer," *IEEE Transactions on Microwave Theory and Techniques*, Vol. 70, No. 5, 2861–2871, May 2022.
[52] Uddin, M. J., M. H. Ullah, and S. Z. Islam, "A broadband polarized metamaterial absorber driven by strong insensitivity and proximity effects," *IEEE Access*, Vol. 9, 131 672–131 684, 2021.
[53] Erkmen, F. and O. M. Ramahi, "A scalable, dual-polarized absorber surface for electromagnetic energy harvesting and wireless power transfer," *IEEE Transactions on Microwave Theory and Techniques*, Vol. 69, No. 9, 4021–4028, September 2021.
[54] Bilal, R. M. H., M. A. Baqir, P. K. Choudhury, M. Karaaslan, M. M. Ali, O. Altlntas, A. A. Rahim, E. Unal, and C. Sabah, "Wideband microwave absorber comprising metallic split-ring resonators surrounded with E-shaped fractal metamaterial," *IEEE Access*, Vol. 9, 5670–5677, 2021.
[55] Yi, J., M. Wei, M. Lin, X. Zhao, L. Zhu, X. Chen, and Z. H. Jiang, "Frequency-tunable and magnitude-tunable microwave metasurface absorbers enabled by shape memory polymers," *IEEE Transactions on Antennas and Propagation*, Vol. 70, No. 8, 6804–6812, August 2022.
[56] Zhang, Y., W. Tang, and B. Lin, "Design of the absorber screen based on the modified bow-tie patch periodical array," in *ISAPE2012*, 269–272, Xi'an, China, October 2012.
[57] Parameswaran, A., A. A. Ovhal, D. Kundu, H. S. Sonalikar, J. Singh, and D. Singh, "A low-profile ultra-wideband absorber using lumped resistor-loaded cross dipoles with resonant nodes," *IEEE Transactions on Electromagnetic Compatibility*, Vol. 64, No. 5, 1758–1766, October 2022.
[58] Zhang, B., C. Jin, and Z. Shen, "Low-profile broadband absorber based on multimode resistor-embedded metallic strips," *IEEE Transactions on Microwave Theory and Techniques*, Vol. 68, No. 3, 835–843, March 2020.
[59] Munk, B. A., P. Munk, and J. Pryor, "On designing Jaumann and circuit analog absorbers (CA absorbers) for oblique angle of incidence," *IEEE Transactions on Antennas and Propagation*, Vol. 55, No. 1, 186–193, January 2007.
[60] Shang, Y., S. Xiao, and Z. Shen, "A thin wideband circuit analog absorber using square-loop arrays," in *2013 IEEE Antennas and Propagation Society International Symposium (APSURSI)*, 472–473, Orlando, FL, USA, July 2013.
[61] Shang, Y., Z. Shen, and S. Xiao, "On the design of single-layer circuit analog absorber using double-square-loop array," *IEEE Transactions on Antennas and Propagation*, Vol. 61, No. 12, 6022–6029, December 2013.
[62] Chen, J., Y. Shang, and C. Liao, "Double-layer circuit analog absorbers based on resistor-loaded square-loop arrays," *IEEE Antennas and Wireless Propagation Letters*, Vol. 17, No. 4, 591–595, April 2018.

[63] Yang, J. and Z. Shen, "A thin and broadband absorber using double-square loops," *IEEE Antennas and Wireless Propagation Letters*, Vol. 6, 388–391, December 2007.
[64] Ghosh, S., S. Bhattacharyya, and K. V. Srivastava, "Design, characterisation and fabrication of a broadband polarisation-insensitive multi-layer circuit analogue absorber," *IET Microwaves, Antennas & Propagation*, Vol. 10, No. 8, 850–855, June 2016.
[65] Han, Y., W. Che, C. Christopoulos, Y. Xiong, and Y. Chang, "A fast and efficient design method for circuit analog absorbers consisting of resistive square-loop arrays," *IEEE Transactions on Electromagnetic Compatibility*, Vol. 58, No. 3, 747–757, June 2016.
[66] Ye, H., W. Che, and C. Christopoulos, "Microwave absorbers made of arrays of square loops with lumped resistors through optimization with genetic algorithm approach," in *2014 XXXIth URSI General Assembly and Scientific Symposium (URSI GASS)*, 1–4, Beijing, China, August 2014.
[67] He, Y., W. Feng, S. Guo, J. Wei, Y. Zhang, Z. Huang, C. Li, L. Miao, and J. Jiang, "Design of a dual-band electromagnetic absorber with frequency selective surfaces," *IEEE Antennas and Wireless Propagation Letters*, Vol. 19, No. 5, 841–845, May 2020.
[68] Yao, Z., S. Xiao, Z. Jiang, L. Yan, and B.-Z. Wang, "On the design of ultrawideband circuit analog absorber based on quasi-single-layer FSS," *IEEE Antennas and Wireless Propagation Letters*, Vol. 19, No. 4, 591–595, April 2020.
[69] Basravi, M., M. Maddahali, Z. H. Firouzeh, and A. Ramezani, "Design of a novel ultra broadband single-layer absorber using double fractal square loops," in *2016 24th Iranian Conference on Electrical Engineering (ICEE)*, 621–625, Shiraz, Iran, May 2016.
[70] Luo, Y., Y. Zhuang, and S. Zhu, "Thin and broadband Salisbury screen absorber using Minkowski fractal structure," in *2009 Asia Pacific Microwave Conference*, 2573–2576, Singapore, December 2009.
[71] Lv, Q., C. Jin, B. Zhang, P. Zhang, J. Wang, N. Kang, and B. Tian, "Wideband dual-polarized microwave absorber at extremely oblique incidence," *IEEE Transactions on Antennas and Propagation*, Vol. 71, No. 3, 2497–2506, March 2023.
[72] Basravi, M., Z. H. Firouzeh, and M. Maddahali, "Design of a single-layer circuit analog absorber using double-circular-loop array via the equivalent circuit model," *Journal of Electrical and Computer Engineering Innovations*, Vol. 5, No. 2, 171–178, 2017.
[73] Yu, J. W., Y. Cai, X. Q. Lin, and X. Wang, "Perforated multi-layer ultrawideband absorber based on circuit analog absorber with optimal air spaces," *IEEE Antennas and Wireless Propagation Letters*, Vol. 19, No. 1, 34–38, January 2020.
[74] Lim, D. and S. Lim, "Ultrawideband electromagnetic absorber using sandwiched broadband metasurfaces," *IEEE Antennas and Wireless Propagation Letters*, Vol. 18, No. 9, 1887–1891, September 2019.
[75] Kundu, D., A. Mohan, and A. Chakrabarty, "Single-layer wideband microwave absorber using array of crossed dipoles," *IEEE Antennas and Wireless Propagation Letters*, Vol. 15, 1589–1592, 2016.
[76] Rashid, A. K., Z. Shen, and S. Aditya, "Wideband microwave absorber based on a two-dimensional periodic array of microstrip lines," *IEEE Transactions on Antennas and Propagation*, Vol. 58, No. 12, 3913–3922, December 2010.
[77] Sohrab, A. P. and Z. Atlasbaf, "A circuit analog absorber with optimum thickness and response in X-band," *IEEE Antennas and Wireless Propagation Letters*, Vol. 12, 276–279, 2013.
[78] Pasupuleti, S., N. R. Palepu, and A. Ghosh, "Design of a broadband microwave absorber for EMI mitigation in wireless communication systems," in *2025 International Conference on Computing, Intelligence, and Application (CIACON)*, 1–6, Durgapur, India, July 2025.
[79] Inbavalli, V. P., V. P. Sakthivel, C. Venkatesh, and T. R. S. Kumar, "Design of broadband circuit analog absorber with optimal thickness for stable angular response in C, X, Ku, and K bands," *IEEE Transactions on Electromagnetic Compatibility*, Vol. 65, No. 6, 2065–2069, December 2023.
[80] Hossain, M. I., N. Nguyen-Trong, K. H. Sayidmarie, and A. M. Abbosh, "Equivalent circuit design method for wideband nonmagnetic absorbers at low microwave frequencies," *IEEE Transactions on Antennas and Propagation*, Vol. 68, No. 12, 8215–8220, December 2020.
[81] Che Seman, F., R. Cahill, and V. F. Fusco, "Salisbury screen with reduced angular sensitivity," *Electronics Letters*, Vol. 45, No. 3, 147–149, January 2009.
[82] Zadeh, A. K. and A. Karlsson, "Capacitive circuit method for fast and efficient design of wideband radar absorbers," *IEEE Transactions on Antennas and Propagation*, Vol. 57, No. 8, 2307–2314, August 2009.
[83] Kazemzadeh, A. and A. Karlsson, "Multilayered wideband absorbers for oblique angle of incidence," *IEEE Transactions on Antennas and Propagation*, Vol. 58, No. 11, 3637–3646, November 2010.
[84] Che Seman, F., R. Cahill, V. F. Fusco, and G. Goussetis, "Design of a Salisbury screen absorber using frequency selective surfaces to improve bandwidth and angular stability performance," *IET Microwaves, Antennas & Propagation*, Vol. 5, No. 2, 149–156, January 2011.
[85] Kazemzade, A., "Nonmagnetic ultrawideband absorber with optimal thickness," *IEEE Transactions on Antennas and Propagation*, Vol. 59, No. 1, 135–140, January 2011.
[86] Li, M., S. Xiao, Y.-Y. Bai, and B.-Z. Wang, "An ultrathin and broadband radar absorber using resistive FSS," *IEEE Antennas and Wireless Propagation Letters*, Vol. 11, 748–751, 2012.
[87] Sun, Z., L. Yan, X. Zhao, and R. X.-K. Gao, "An ultrawideband frequency selective surface absorber with high polarization-independent angular stability," *IEEE Antennas and Wireless Propagation Letters*, Vol. 22, No. 4, 789–793, April 2023.
[88] Ye, H. and W. Che, "Analysis and design of a Salisbury screen absorber with High Impedance Ground Plane," in *2013 Cross Strait Quad-Regional Radio Science and Wireless Technology Conference*, 325–328, Chengdu, China, July 2013.
[89] Sudhendra, C., A. R. Madhu, A. C. R. Pillai, R. Kark, and T. S. Rukmini, "A novel ultra wide band radar absorber based on hexagonal resistive patch FSS," in *2013 IEEE Applied Electromagnetics Conference (AEMC)*, 1–2, Bhubaneswar, India, December 2013.
[90] Choi, W.-H., J.-H. Shin, T.-H. Song, J.-B. Kim, C.-M. Cho, and W.-J. Lee, "Design of circuit-analog (CA) absorber and application to the leading edge of a wing-shaped structure," *IEEE Transactions on Electromagnetic Compatibility*, Vol. 56, No. 3, 599–607, June 2014.
[91] Tang, W., G. Goussetis, H. Legay, and N. J. G. Fonseca, "Efficient synthesis of low-profile angularly-stable and polarization-independent frequency-selective absorbers with a reflection band," *IEEE Transactions on Antennas and Propagation*, Vol. 63, No. 2, 621–629, February 2015.
[92] Zabri, S. N., R. Cahill, and A. Schuchinsky, "Compact FSS absorber design using resistively loaded quadruple hexago-

nal loops for bandwidth enhancement," *Electronics Letters*, Vol. 51, No. 2, 162–164, January 2015.

[93] Bhati, A., K. R. Hiremath, and V. Dixit, "Design and characterization of square patch Salisbury screen microwave absorber," *Progress In Electromagnetics Research Letters*, Vol. 76, 7–12, 2018.

[94] Firouzfar, A., M. Afsahi, and A. A. Orouji, "Novel synthesis formulas to design square patch frequency selective surface absorber based on equivalent circuit model," *International Journal of RF and Microwave Computer-Aided Engineering*, Vol. 29, No. 6, e21680, February 2019.

[95] Seman, F. C., S. Omar, F. A. Poad, W. Y. Yong, S. K. A. Rahim, E. Baharudin, and S. M. Shah, "Phase characteristics of multi-layer crossed-dipole FSS in salisbury screen absorber," in *2018 IEEE International RF and Microwave Conference (RFM)*, 356–358, Penang, Malaysia, December 2018.

[96] Hou, J., H. Lin, W. Xu, Y. Tian, Y. Wang, X. Shi, F. Deng, and L. Chen, "Customized inverse design of metamaterial absorber based on target-driven deep learning method," *IEEE Access*, Vol. 8, 211 849–211 859, 2020.

[97] Wu, C., S. Lu, Z. Yang, and Y. Yashchyshyn, "A UWB absorber based on the TCA concept in the UHF band," *IEEE Transactions on Antennas and Propagation*, Vol. 68, No. 5, 4132–4136, May 2020.

[98] Deng, G., L. Wang, J. Sun, J. Yang, Z. Yin, Y. Li, W. Zhang, and Z. Li, "Ultra-broadband and wide angularly stable electromagnetic wave absorber based on multilayer resistive films for RCS reduction," *IEEE Transactions on Electromagnetic Compatibility*, Vol. 67, No. 2, 449–458, April 2025.

[99] Costa, F., A. Monorchio, and G. Manara, "Analysis and design of ultra thin electromagnetic absorbers comprising resistively loaded high impedance surfaces," *IEEE Transactions on Antennas and Propagation*, Vol. 58, No. 5, 1551–1558, May 2010.

[100] Kim, J., H.-K. Jang, J. Oh, and J. Park, "A rational design procedure for absorbers of square-loop-shaped resistive frequency selective surface placed on glass/epoxy laminate," *IEEE Transactions on Electromagnetic Compatibility*, Vol. 65, No. 1, 104–113, February 2023.

[101] Gao, M., Q. Chen, Y. Zheng, L. Ding, D. Liao, and Y. Fu, "Ultrabroadband absorber based on layered inkjet-printing resistive film," *IEEE Antennas and Wireless Propagation Letters*, Vol. 22, No. 2, 228–232, February 2023.

[102] Dhumal, A., M. S. Bisht, A. Bhardwaj, M. Saikia, S. Malik, and K. V. Srivastava, "Screen printed polarization independent microwave absorber for wideband RCS reduction," *IEEE Transactions on Electromagnetic Compatibility*, Vol. 65, No. 1, 96–103, February 2023.

[103] Singh, A. and N. Gupta, "Screen-printed wideband absorber for the X and Ku bands," *IEEE Transactions on Electromagnetic Compatibility*, Vol. 64, 1321–1329, October 2022.

[104] Li, Y., P.-F. Gu, Z. He, Z. Cao, J. Cao, K. W. Leung, and D. Ding, "An ultra-wideband multilayer absorber using an equivalent circuit-based approach," *IEEE Transactions on Antennas and Propagation*, Vol. 70, 11 911–11 921, December 2022.

[105] Huang, X., M. Lin, Z. Wu, K. Cheng, T. Tian, D. Guan, *et al.*, "Screen overprinted flexible radar absorber composed of planar resistor loaded metamaterials," *IEEE Antennas and Wireless Propagation Letters*, Vol. 19, No. 8, 1281–1285, August 2020.

[106] Choi, W.-W., S. Baek, S.-W. Kim, T. Choi, H. J. Lee, I. Kim, S. Koh, J.-G. Yook, and K. Kim, "Metasurface embedded microwave absorbing composites on curved surfaces for radar cross section reduction," *IEEE Access*, Vol. 13, 179 463–179 474, 2025.

[107] Chou, H.-T. and Y.-S. Chang, "Statistical analysis of fabrication discrepancy effects on periodic circuit analog electromagnetic absorbers," *IEEE Transactions on Electromagnetic Compatibility*, Vol. 63, 410–418, April 2021.

[108] David, V., I. Nica, and A. Salceanu, "Electromagnetic absorbers based on chiral honeycomb slab," in *2009 International Symposium on Electromagnetic Compatibility — EMC Europe*, 1–4, Athens, Greece, June 2009.

[109] Yuan, Q., S. Qu, H. Ma, S. Sui, Y. Shen, J. Wang, M. Feng, H. Chen, Y. Jin, and X. Wang, "A broadband wide-angle synthetical absorber designed by topology optimization of resistance surface and metal wires," *IEEE Access*, Vol. 7, 142 675–142 681, 2019.

[110] Luo, G. Q., W. Yu, Y. Yu, X. H. Zhang, and Z. Shen, "A three-dimensional design of ultra-wideband microwave absorbers," *IEEE Transactions on Microwave Theory and Techniques*, Vol. 68, 4206–4215, October 2020.

[111] Shi, T., L. Jin, L. Han, M.-C. Tang, H.-X. Xu, and C.-W. Qiu, "Dispersion-engineered, broadband, wide-angle, polarization-independent microwave metamaterial absorber," *IEEE Transactions on Antennas and Propagation*, Vol. 69, No. 1, 229–238, January 2021.

[112] Xue, K., H. Zhai, S. Li, and Y. Shang, "A miniaturized absorber frequency selective surface with good angular stability," *IEEE Antennas and Wireless Propagation Letters*, Vol. 19, 24–28, January 2020.

[113] Yu, J., W. Jiang, and S. Gong, "Wideband angular stable absorber based on spoof surface plasmon polariton for RCS reduction," *IEEE Antennas and Wireless Propagation Letters*, Vol. 19, No. 7, 1058–1062, July 2020.

[114] Laur, V., A. Maalouf, A. Chevalier, and F. Comblet, "Three-dimensional printing of honeycomb microwave absorbers: Feasibility and innovative multiscale topologies," *IEEE Transactions on Electromagnetic Compatibility*, Vol. 63, No. 2, 390–397, April 2021.

[115] Wu, X., C. Fu, C. Feng, J. Gao, W. Chu, X. Zhu, W. Gu, D. Sun, Y. Yue, and W. Wu, "Stretchable broadband absorbers based on the hauberk structure," *IEEE Antennas and Wireless Propagation Letters*, Vol. 22, No. 3, 467–471, March 2023.

[116] Naik, K. H. M., A. K. Singh, and D. R. Krishna, "Additively manufactured 3-D printed ultra wideband polarization insensitive absorber," in *2025 Third International Conference on Microwave, Antenna and Communication (MAC)*, 1–4, Bhopal, India, June 2025.

[117] Grande, M., A. D'Orazio, G. V. Bianco, G. Bruno, M. A. Vincenti, D. d. Ceglia, and M. Scalora, "Optically transparent graphene-based Salisbury screen microwave absorber," in *2015 IEEE 15th Mediterranean Microwave Symposium (MMS)*, 1–3, Lecce, Italy, November 2015.

[118] Motevasselian, A. and B. L. G. Jonsson, "A partially transparent Jaumann absorber applied to an aircraft wing profile," in *2010 IEEE Antennas and Propagation Society International Symposium*, 1–4, Toronto, ON, Canada, July 2010.

[119] Sheokand, H., G. Singh, S. Ghosh, J. Ramkumar, S. A. Ramakrishna, and K. V. Srivastava, "An optically transparent broadband microwave absorber using interdigital capacitance," *IEEE Antennas and Wireless Propagation Letters*, Vol. 18, No. 1, 113–117, January 2019.

[120] Li, Y., Z. Sun, and E.-P. Li, "Design and analysis of a miniaturized broadband resistive film absorber to reduce chip system radiation," *IEEE Transactions on Electromagnetic Compatibil-*

ity, Vol. 65, No. 3, 749–760, June 2023.

[121] Gupta, N. K., G. Singh, S. Srinivasu, H. Wanare, K. V. Srivastava, J. Ramkumar, and S. A. Ramakrishna, "Singular phase characteristics of electromagnetic absorbers and a framework for low-RCS target detection," *IEEE Antennas and Wireless Propagation Letters*, Vol. 22, No. 1, 134–138, Jan. 2023.

[122] Wu, Y., C. Fu, S. Qian, Z. Zong, X. Wu, Y. Yue, and W. Gu, "Flexible and transparent W-band absorber fabricated by EHD printing technology," *IEEE Antennas and Wireless Propagation Letters*, Vol. 19, No. 8, 1345–1349, August 2020.

[123] Zhang, L., Y. Shi, J. X. Yang, X. Zhang, and L. Li, "Broadband transparent absorber based on indium tin oxide-polyethylene terephthalate film," *IEEE Access*, Vol. 7, 137 848–137 855, 2019.

[124] Li, Y., Y. Wu, D. Li, M. Zhu, Y. Qiu, G. Yu, and E. Li, "A miniaturized perfect metamaterial absorber for EMI radiation suppression," *IEEE Transactions on Electromagnetic Compatibility*, Vol. 66, No. 3, 776–786, June 2024.

[125] Wu, R., J. Dong, C. Xiao, H. Dou, S. Zhang, C. Zhang, and M. Tian, "An optically transparent broadband metamaterial absorber for passive radiation jamming," *IEEE Transactions on Microwave Theory and Techniques*, Vol. 73, No. 11, 8607–8618, November 2025.

[126] Wang, Q., K. Bi, and S. Lim, "All-dielectric transparent metamaterial absorber with encapsulated water," *IEEE Access*, Vol. 8, 175 998–176 004, 2020.

[127] Inbavalli, V. P., T. R. SureshKumar, and C. A. Zachariah, "Indium tin oxide based optically transparent wide band flexible circuit analog absorber for optical window applications," in *2023 Joint Asia-Pacific International Symposium on Electromagnetic Compatibility and International Conference on ElectroMagnetic Interference & Compatibility (APEMC/INCEMIC)*, 1–4, Bengaluru, India, May 2023.

[128] Chambers, B. and A. Tennant, "The phase-switched screen," *IEEE Antennas and Propagation Magazine*, Vol. 46, No. 6, 23–37, December 2004.

[129] Chambers, B., "Frequency tuning characteristics of capacitivelyloadedsalisbury screen radar absorber," *Electronics Letters*, Vol. 30, No. 19, 1626–1628, September 1994.

[130] Luo, Z., X. Shan, X. Ren, K. Wu, Y. Chen, and L. Hong, "Active metasurface absorber for intensity-dependent surface-wave shielding," *IEEE Transactions on Antennas and Propagation*, Vol. 71, No. 7, 5795–5804, July 2023.

[131] Tennant, A. and B. Chambers, "Adaptive radar absorbing structure with PIN diode controlled active frequency selective surface," *Smart Materials and Structures*, Vol. 13, No. 1, 122–125, December 2003.

[132] Seman, F. C., R. Cahill, and V. F. Fusco, "Electronically tunable liquid crystal based Salisbury screen microwave absorber," in *2009 Loughborough Antennas & Propagation Conference*, 93–96, Loughborough, UK, November 2009.

[133] Ghosh, S. and K. V. Srivastava, "A polarization-independent broadband multilayer switchable absorber using active frequency selective surface," *IEEE Antennas and Wireless Propagation Letters*, Vol. 16, 3147–3150, 2017.

[134] Fan, Y., D. Li, H. Ma, J. Xing, Y. Gu, L. K. Ang, and E.-P. Li, "Ultrawideband dual-polarized frequency-selective absorber with tunable reflective notch," *IEEE Transactions on Antennas and Propagation*, Vol. 71, No. 3, 2855–2860, March 2023.

[135] Fu, C., L. Zhang, L. Liu, S. Dong, W. Yu, and L. Han, "RCS reduction on patterned graphene-based transparent flexible metasurface absorber," *IEEE Transactions on Antennas and Propagation*, Vol. 71, No. 2, 2005–2010, February 2023.

[136] Zhao, B., C. Huang, J. Yang, J. Song, C. Guan, and X. Luo, "Broadband polarization-insensitive tunable absorber using active frequency selective surface," *IEEE Antennas and Wireless Propagation Letters*, Vol. 19, No. 6, 982–986, June 2020.

[137] Liu, X., X. Chen, L. Han, J. Su, R. Ma, and W. Zhang, "Dual-band energy-selective surface with wide absorption band," *IEEE Transactions on Microwave Theory and Techniques*, Vol. 73, No. 12, 10 241–10 249, December 2025.

[138] Zhang, Y., Z. Cao, Z. Huang, L. Miao, S. Bie, and J. Jiang, "Ultrabroadband double-sided and dual-tuned active absorber for UHF band," *IEEE Transactions on Antennas and Propagation*, Vol. 69, No. 2, 1204–1208, February 2021.

[139] Yu, M., H. Wang, X. Gao, X. Ren, Z. Tian, H. Ding, and Z. Hou, "Reconfigurable plasma composite absorber coupled with pixelated frequency selective surface generated by FD-CGAN," *IEEE Access*, Vol. 11, 3914–3925, 2023.

[140] Zhang, Q., Z. Shen, J. Wang, and K. S. Lee, "Design of a switchable microwave absorber," *IEEE Antennas and Wireless Propagation Letters*, Vol. 11, 1158–1161, 2012.

[141] Geng, M.-Y., Z.-G. Liu, W.-J. Wu, H. Chen, B. Wu, and W.-B. Lu, "A dynamically tunable microwave absorber based on graphene," *IEEE Transactions on Antennas and Propagation*, Vol. 68, No. 6, 4706–4713, June 2020.

[142] Song, J., C. Huang, J. Yang, X. Zhang, J. Peng, and X. Luo, "Broadband and tunable radar absorber based on graphene capacitor integrated with resistive frequency-selective surface," *IEEE Transactions on Antennas and Propagation*, Vol. 68, No. 3, 2446–2450, March 2020.

[143] Xing, B.-B., Z.-G. Liu, W.-B. Lu, H. Chen, and Q.-D. Zhang, "Wideband microwave absorber with dynamically tunable absorption based on graphene and random metasurface," *IEEE Antennas and Wireless Propagation Letters*, Vol. 18, No. 12, 2602–2606, December 2019.

[144] Zhou, M.-J., F. Ding, S.-N. Yu, X.-J. Yuan, X.-Z. Ye, Y.-T. Liu, W.-B. Sun, H.-L. Yuan, and M. Chen, "A tunable electromagnetic wave absorber for uniform reflection modulation in broadband," *Journal of Applied Physics*, Vol. 137, No. 12, 123106, March 2025.

[145] Hao, X. J., X. Q. Lin, X. M. Yang, Y. H. Su, Y. Yao, and Y. L. Yang, "Dual-polarized dual-band-notched frequency-selective absorber with high design freedom," *IEEE Antennas and Wireless Propagation Letters*, Vol. 22, No. 1, 59–63, January 2023.

[146] Rahman, S. U., Q. Cao, M. A. Akbar, A. Alsanad, A. Gumaei, and Y. Wang, "An integrated switchable EM absorber and beam switchable radiator," *IEEE Access*, Vol. 8, 193 050–193 059, 2020.

[147] Shahsavaripour, A., M. H. Badiei, A. Kalhor, and L. Yousefi, "Design of thin, wideband electromagnetic absorbers with polarization and angle insensitivity using deep learning," *Scientific Reports*, Vol. 15, No. 1, 9426, March 2025.

[148] On, H.-I., L. Jeong, T.-M. Seo, Y. Jo, W. Choi, D.-J. Kang, J.-H. Park, and H.-J. Lee, "Novel method of performance-optimized metastructure design for electromagnetic wave absorption in specific band using deep learning," *Engineering Applications of Artificial Intelligence*, Vol. 137, 109274, November 2024.

[149] Garg, P., "Design and optimization of a metamaterial absorber using machine learning models," *Journal of Electronic Materials*, Vol. 55, No. 1, 790–799, November 2025.

[150] Orasugh, J. T., A. Mohanty, A. Malakar, S. Bose, and S. S. Ray, "Design and applications of multi-frequency programmable metamaterials for adaptive stealth," *Advanced Functional Materials*, Vol. 36, No. 5, e13726, January 2026.

[151] Kossifos, K. M., L. Petrou, G. Varnava, A. Pitilakis, O. Tsilipakos, F. Liu, P. Karousios, A. C. Tasolamprou, M. Seckel, D. Manessis, N. V. Kantartzis, D.-H. Kwon, M. A. Antoniades, and J. Georgiou, "Toward the realization of a programmable metasurface absorber enabled by custom integrated circuit technology," *IEEE Access*, Vol. 8, 92 986–92 998, May 2020.

[152] Deng, G., L. Wang, B. Chi, H. Fang, J. Sun, Y. Li, J. Yang, and Z. Yin, "Block building architecture for a multifunctional broadband electromagnetic wave absorber based on the free-standing resistive film," *ACS Applied Electronic Materials*, Vol. 5, No. 8, 4587–4594, July 2023.